Organic & Biomolecular Chemistry

ROYAL SOCIETY OF CHEMISTRY

COMMUNICATION

View Article Online
View Journal | View Issue

Open Access Article. Published on 21 December 2022. Downloaded on 2/8/2026 4:38:49 PM.
This article is licensed under a Creative Commons Attribution-NonCommercial 3.0 Unported Licence.

Check for updates

Cite this: *Org. Biomol. Chem.*, 2023, **21**, 743

Received 15th November 2022,
Accepted 20th December 2022

DOI: 10.1039/d2ob02088b

rsc.li/obc

Exploiting multivalency and cooperativity of gold nanoparticles for binding phosphatidylinositol (3,4,5)-trisphosphate at sub-nanomolar concentrations†

Flavio della Sala,[a,b] Elisa Ceresara,[a] Fabrizio Micheli,[c] Stefano Fontana,[c] Leonard J. Prins *[a] and Paolo Scrimin *[a]

Cationic, monolayer-protected gold nanoparticles provide a multivalent charged surface and a hydrophobic monolayer that synergistically contribute to the binding of phosphatidylinositol (3,4,5)-trisphosphate, a relevant biomarker. The observed dissociation constant is in the picomolar region, providing the possibility of using these gold nanoparticles for the selective extraction of this molecule from biological fluids.

Clusters of gold(0) atoms of nanometer size are easily passivated by thiols, thus forming monolayer-protected gold nanoparticles (AuNPs).[1] By suitably coding the structure of the passivating thiols, the surface and the monolayer of AuNPs can be easily tuned to obtain nanomaterials with many properties[2] ranging from molecular recognition of the most diverse substrates to their transformation. This led, for instance, to the development of "nanosensors"[3] or "nanozymes".[4–6] The latter are AuNP-based catalysts mimicking the properties of natural enzymes.[7] In analogy to biological membranes, the binding of substrates to monolayer-functionalized AuNPs relies on a concurrent and concerted combination of electrostatic and hydrophobic interactions, hydrogen bonds and, if present, coordination to metal ions. In this contribution we show how dissociation constants in the picomolar concentration region can be easily attained by taking advantage of concurrent ionic/coordination and hydrophobic interactions with a multivalent system constituted by monolayer passivated gold nanoparticles. More importantly, we show how they can be exploited for the binding of a relevant biomarker.

A previous study with minimalist, small AuNPs, passivated with thiols terminated with 1,4,7-triazacyclononane (TACN) (such as AuNP **1**·Zn^{II} in Fig. 1), has shown that the affinity of dimethyl phosphate (DMP) for those nanoparticles is relatively low (K_d = 3.8 × 10^{-3} M, entry 1 of Table 1)[8] but the conjugation with a nucleobase brings it down to 1.2 × 10^{-4} M (cAMP, see Fig. 1 and entry 4 of Table 1).[9] In such a molecule, the interaction with the cationic metal complexes located on the

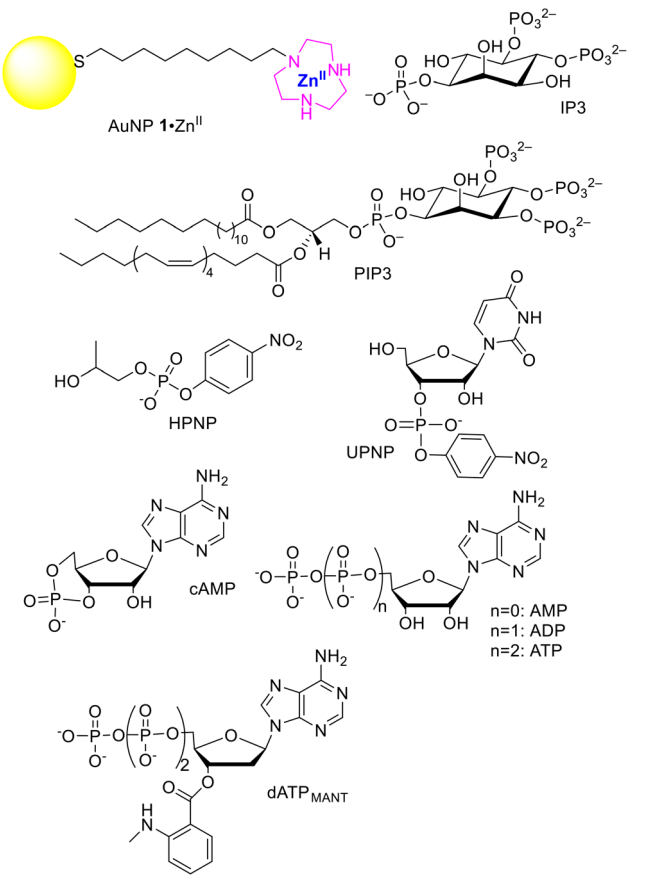

Fig. 1 Compounds discussed in this work (counterions have been omitted for clarity).

[a]*University of Padova, Department of Chemical Sciences, via Marzolo, 1 35131 Padova, Italy. E-mail: leonard.prins@unipd.it, paolo.scrimin@unipd.it*
[b]*Department of Chemistry, University of Manchester, M13 9LP, UK*
[c]*Aptuit (Verona) Srl, an Evotec company, Campus Levi-Montalcini, Via Alessandro Fleming 4, 37135 Verona, Italy*

†Electronic supplementary information (ESI) available. See DOI: https://doi.org/10.1039/d2ob02088b

Open Access Article. Published on 21 December 2022. Downloaded on 2/8/2026 4:38:49 PM.
This article is licensed under a Creative Commons Attribution-NonCommercial 3.0 Unported Licence.

Table 1 Dissociation constants of the compounds shown in Fig. 1 from the Zn^{II} complexes of gold nanoparticles

Entry	Substrate	K_d,[a] M	Rel. K_d [b]	Ref.
1	DMP	3.8×10^{-3} [c]	1	8
2	HPNP	5.8×10^{-4} [c]	6.6	8
3	UPNP	3.0×10^{-5} [d]	1.3×10^{2}	12
4	cAMP	1.2×10^{-4} [e]	32.8	9
5	AMP	7.3×10^{-6} [e]	5.3×10^{3}	9
6	ADP	1.8×10^{-7} [e]	2.1×10^{4}	9
7	ATP	$<1.8 \times 10^{-7}$ [e,f]	1.1×10^{5}	9
8	$dATP_{MANT}$	3.2×10^{-11} [g]	1.2×10^{8}	19
9	PIP3	2.9×10^{-11} [h]	1.3×10^{8}	This work
10	IP3	$>2 \times 10^{-8}$ [h,i]	—	This work

[a] All measurements have been performed at least in triplicate. The error in the dissociation constants of entries 1–6 is lower than 7%; the value of entry 8 is an estimate as the correct value is likely 1 order of magnitude lower; the error in entry 9 is 6%; the reported value of entry 10 is an estimate as the correct value is likely slightly higher. [b] $K_{d,DMP}/K_d$. [c] At 40 °C, pH = 7.5. [d] At 25 °C, pH = 7.5. [e] At 40 °C, pH = 7; data were corrected for the concentration of the probe to allow comparison with the other substrates; details are reported in the ESI.† [f] The exact value could not be determined because of the experimental conditions. [g] At 25 °C, pH = 7. [h] At 37 °C, pH = 7.5. [i] Estimated value.

surface of the monolayer is driven not only by the phosphate group but also by the adenine moiety, although more weakly.[10] A contribution similar in strength to that of adenine but relying on different interactions can be provided by a hydrophobic residue. In fact, hydroxypropyl-*p*-nitrophenyl phosphate (HPNP, Fig. 1), a phosphate diester often used as a model of RNA in hydrolytic studies and devoid of the nucleobase, presents only a slightly higher dissociation constant than cAMP (5.8×10^{-4} M, see entry 2 of Table 1).[8] The hydrophobic contribution is derived from the *p*-nitrophenyl moiety. The addition to HPNP of uracil as in UPNP (Fig. 1), a nucleobase binding more strongly than adenine to the Zn(II) complex,[11] contributes to bringing down the dissociation constant by *ca.* 20-fold (3.0×10^{-5} M, see entry 3 of Table 1).[12] The study of cAMP siblings where the charge was increased up to −4 (see Fig. 1 and entries 5–7 of Table 1) showed that the dissociation constant decreased by more than two orders of magnitude by doubling the charge (from cAMP to AMP) but only by 5-fold with each subsequent charge increase (from AMP to ADP and, possibly, ATP) down to less than 1.8×10^{-7} M (ADP and even less for ATP).[9] Likely geometrical strain or non-optimal complementarity of the polyanions with the metal ions present on the nanoparticle surface leads to a lower increase in binding strength.[13] This high affinity constant led to the selective detection of these phosphates by using these metal AuNPs,[14–16] and their extraction from complex mixtures.[17,18] It has been estimated that DNA binds to such nanoparticles at concentrations well below the nanomolar range.[7] The very high affinity takes advantage of the polyvalent nature of both the nanoparticle surface and the target molecule leading to a Velcro-like interaction. By exploiting coordination, hydrophobic and nucleobase interactions, the fluorescent probe 2′-deoxy-3′-*O*-(*N*′-methylanthraniloyl)adenosine-5′-*O*-triphosphate ($dATP_{MANT}$, Fig. 1) shows the strongest binding to these AuNPs with a dissociation constant of *ca.* 3.2×10^{-11} M (entry 8 of Table 1).[19]

Following the above experimental evidence, it occurred to us that these AuNPs, by exploiting their multivalency and taking advantage of such concurrent interactions, could strongly bind to relevant biological targets. The example we will consider here is the hydrophobic polyanionic molecule 1-stearoyl-2-arachidonyl-*sn-glycero*-3-phospho-(1′-*myo*-inositol-3′,4′,5′-triphosphate) (PIP3, Fig. 1). PIP3 is characterized by a polyanionic headgroup (formal charge −7, but more likely −4/−5 under the operating conditions[20])‡ and two lipophilic fatty acid chains connected to it. It belongs to a low-abundant class of cell membrane phospholipids (phosphoinositides, PIs).[21] Although they constitute less than 0.05% of the total cellular phospholipids, they are key regulators of several fundamental cellular processes.[22] Alteration of PI metabolism is often involved in pathological states,[23] thus making PIs valuable targets for diagnostic and therapeutic applications. For the monolayer, we used that provided by gold nanoparticles AuNP **1**·Zn^{II} (Fig. 1), with a diameter of 1.5 ± 0.3 nm (Fig. S1†). We used small nanoparticles to maximize the [ligand]/[Au] ratio and to compare our data with previous ones available from the literature.

The strength of the interaction with PIP3 was studied by means of a competition experiment monitoring the fluorescence change (λ_{ex} = 355 nm, λ_{em} = 428 nm) of the probe $dATP_{MANT}$ (see above). The experiment relies on probe displacement from the nanoparticle monolayer where the fluorescence is quenched, resulting in an increase in fluorescence intensity (ESI, Fig. S2†). The high affinity of $dATP_{MANT}$ for these AuNPs represents a quite challenging benchmark for PIP3.

We operated at the surface saturation concentration (SSC) of $dATP_{MANT}$ to ensure that any binding event of PIP3 to the monolayer would result in the release of the fluorophore. The SSC of $dATP_{MANT}$ for AuNP **1**·Zn^{II} was determined to be 3.3 ± 0.1 μM under the experimental conditions we used (ESI, Fig. S2 and 3†). Together with PIP3, we also screened D-*myo*-inositol-1,4,5-triphosphate (IP3) with a similar anionic moiety (the charge is expected to be −4 under the operating conditions[20]),‡ but devoid of the lipophilic tails. It is involved in signal transduction pathways for the intracellular release of calcium ions.[24] Fig. 2a shows the increase of florescence when we added PIP3 and IP3 (up to 10 μM) to a buffered solution (HEPES, pH 7.0, 10 mM) containing a mixture of AuNP **1**·Zn^{II} (10 μM in the metal complex) and probe $dATP_{MANT}$ (3.3 μM, 100% SSC). We set the temperature at 37 °C to replicate the physiological conditions. Fluorescence experiments with the probe 1,6-diphenylhexa-1,3,5-triene (DPH) allowed us to assess that the critical aggregation concentration (CAC) of PIP3, which is an amphiphile, is *ca.* 10.5 μM under the experimental conditions (Fig. S4 of the ESI†). Accordingly, significant PIP3 aggregation is observed only at [PIP3] > 10.5 μM, and at 10 μM (the maximum PIP3 concentration used in our experiments), it is still mostly a monomeric, non-aggregated molecule. The response of the probe conjugated AuNPs to the two PIs was

 This journal is © The Royal Society of Chemistry 2023

Open Access Article. Published on 21 December 2022. Downloaded on 2/8/2026 4:38:49 PM.
This article is licensed under a Creative Commons Attribution-NonCommercial 3.0 Unported Licence.

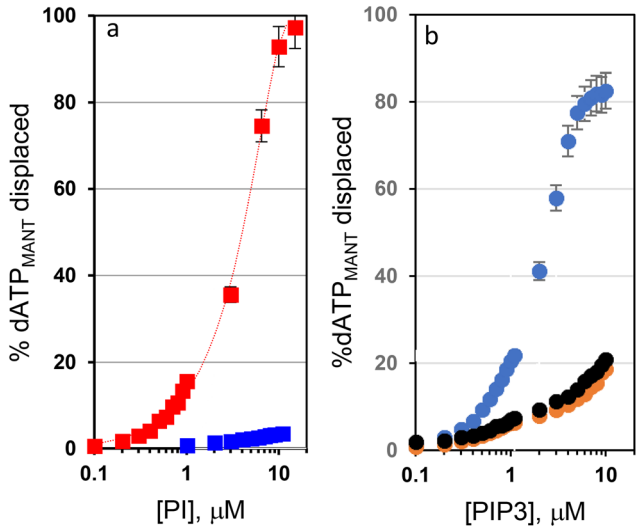

Fig. 2 (a) Displacement of the fluorescent probe dATP$_{MANT}$ (3.3 μM) at 37 °C in pH 7.0 HEPES buffer (10 mM) from the surface of AuNP **1**·Zn^{II} (10 μM, in the metal complex) as a function of the concentration of PIP3 (red squares) and IP3 (blue squares). (b) The same experiment but using only PIP3 and simulated lung fluids (SLF1, blue; SLF3, orange; SLF4, black). [dATP$_{MANT}$] = 1.0 μM; all other conditions are identical. Error bars are derived from at least three independent experiments and are visible only for points at the highest concentrations as the others are within the size of the symbols.

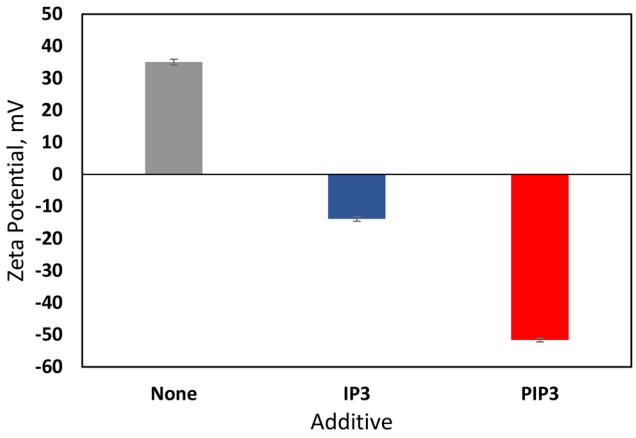

Fig. 3 Zeta potentials obtained for AuNP **1**·Zn^{II} (10 μM in 10 mM pH 7.0 HEPES buffer) without and with the addition of IP3 or PIP3 (10 μM). Errors are derived from triplicate experiments.

quite different (Fig. 2a, and Fig. S5 of the ESI†). While IP3 (at the maximum concentration studied, 10 μM) was unable to displace more than 5% of probe dATP$_{MANT}$, PIP3 gave a well-behaved binding isotherm with total displacement of dATP$_{MANT}$ from the nanoparticle surface.

The IC$_{50}$ of PIP3 with the nanoparticle surface determined in the competition experiment was 3.0 μM.

Since the estimated dissociation constant of dATP$_{MANT}$ for AuNP **1**·Zn^{II} was 3.2 × 10^{-11} M (entry 8 of Table 1), the dissociation constant calculated for PIP3 was 2.9 × 10^{-11} M, a rather impressive value. This confirmed our initial hypothesis that the hydrophobic tails of PIP3 play a very important role in its interaction with AuNP **1**·Zn^{II} even in the absence of the nucleobase (which is present in dATP$_{MANT}$).

With the aim of differentiating the contribution to the binding of the PIs derived from the interaction with the metal complexes on the surface and the hydrophobic one within the monolayer, we determined the zeta potential of the nanoparticles before and after the addition of PIP3 and IP3 (Fig. 3). These experiments were performed in the absence of the florescence probe, thus only PIP3 or IP3 interacted with AuNP **1**·Zn^{II}. The zeta potential determines the charge present at the interface between the nanoparticle surface (actually its slipping plane) and the solvent.[25,26] Native AuNP **1**·Zn^{II} (10 μM in 10 mM pH 7.0 HEPES buffer) gave a positive zeta potential (+35.0 ± 0.9 mV) in line with the highly positive charge of the nanoparticle surface to which the counterions (NO_3^-, buffer) are weakly bound. Addition of IP3 or PIP3 (10 μM) brought down the zeta potential to −13.9 ± 0.7 and −51.7 ± 0.6 mV, respectively. The slightly negative value observed with IP3 indicates that it interacts with the surface more tightly than the nitrate counterions, likely taking advantage of the multivalent interactions between the phosphate groups and the metal ions. The highly negative zeta potential obtained after the addition of PIP3 indicates that far more molecules are tightly bound to the nanoparticles than in the case of simple coordination to the metal complexes (like in the case of IP3). This "excess" of bound molecules is the result of the additional hydrophobic interactions that contribute to the tight binding of PIP3 to the passivating monolayer. Notably, the binding of PIP3 to the nanoparticles also induces an increase of their size (Fig. S1†).

The solvent we used was rather user friendly compared to more demanding environments, like those found in biological samples. We thus focused our attention to the standard, simulated lung fluids (SLFs).[27] SLFs are commonly used to mimic the bronchoalveolar lavage fluid, which is the biological matrix in which PIP3 is typically quantified. Specifically, the composition of SLFs we used (Table S1†) resembles the artificial lysosomal fluids. They differ in pH, ionic strength, and the presence of additional lipids to mimic different regions of the lungs. We calculated again the SSC of probe dATP$_{MANT}$ for AuNP **1**·Zn^{II}. The SSC values were lower than those calculated in pure buffer (0.9 ± 0.1 μM, 1.1 ± 0.2 μM and 1.0 ± 0.1 μM, respectively, for SLF1, SLF3 and SLF4, Fig. S6 and 7†). Competition experiments could be performed at a lower probe dATP$_{MANT}$ concentration (1 μM for all SLFs) and the profile shown in Fig. 2b was obtained. The results indicate that the interaction of PIP3 with AuNP **1**·Zn^{II} is still very strong in SLF1, but decreases in SLF3 and SLF4 (only 18% of dATP$_{MANT}$ was replaced with 10 μM PIP3). Likely the higher ionic strength (SLF3 and SLF4) and the presence of additional lipids (SLF4) affect the binding.

An indication of the possibility to remove PIP3 quantitatively from solution by using AuNP **1**·Zn^{II} was provided by the ^{31}P-NMR experiments shown in Fig. 4. A solution of AuNP

Open Access Article. Published on 21 December 2022. Downloaded on 2/8/2026 4:38:49 PM.
This article is licensed under a Creative Commons Attribution-NonCommercial 3.0 Unported Licence.

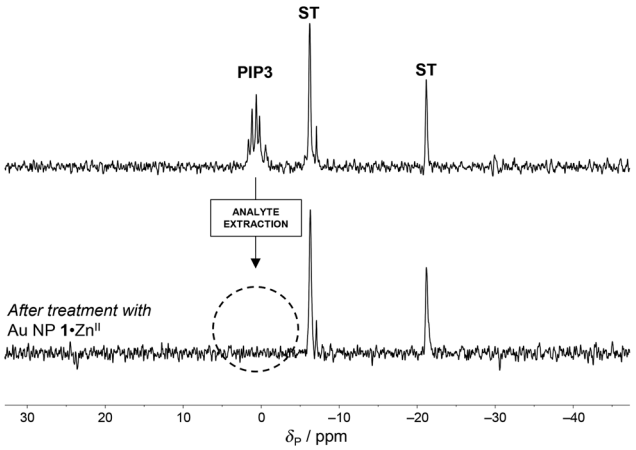

Fig. 4 ^{31}P NMR spectra (10% D_2O, 202 MHz, 300 K) of a buffered solution of PIP3 (0.5 mM, top) before and after co-precipitation with AuNP **1**·Zn^{II} (0.5 mM, in the metal complex, bottom). Experimental conditions: [$Na_5P_3O_{10}$] = 5 mM (external standard, ST), [HEPES, pH 7.0] = 10 mM.

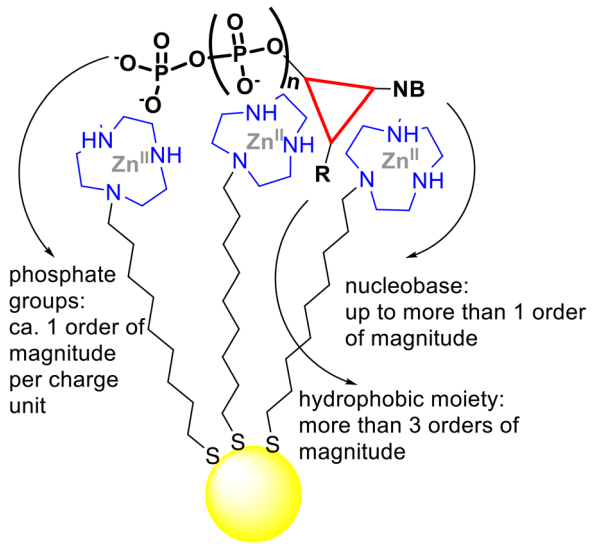

Fig. 5 Pictorial representation of the incremental contribution to the binding of a multivalent substrate to the multivalent Zn^{II}-functionalized monolayer of AuNPs. These incremental gains are largely derived from the entropic advantage resulting from the binding of two multivalent species.

1·Zn^{II} (0.5 mM in the metal complex) and PIP3 (0.5 mM) in buffer (HEPES, pH 7.0, 10 mM) was let to equilibrate. Afterwards, the precipitation of the nanoparticles was induced by adding diethyl ether (28%).§ Removal of the precipitate by centrifugation and analysis of the solvent revealed complete disappearance of the resonances corresponding to PIP3, showing that, within the sensibility of ^{31}P-NMR, AuNP **1**·Zn^{II} completely removed PIP3 from the solution.[28] This could suggest a possible application of AuNP **1**·Zn^{II} in the quantitative extraction of PIP3 from biological fluids.[29]

In conclusion, we have shown that small gold nanoparticles passivated with hydrophobic thiols terminated with a Zn^{II} complex interact very strongly with the relevant cell membrane phospholipid PIP3. The calculated dissociation constant is *ca.* 29 pM. Table 1 very clearly shows how the dissociation constant of a substrate from the monolayer of nanoparticles such as AuNP **1**·Zn^{II} (or very similar ones) decreases progressively from mM (DMP, entry 1) to pM (PIP3, entry 9). Thus, if we consider as our reference the monoanionic, poorly lipophilic substrate DMP that cannot exploit multivalency, we observe that the affinity constant for PIP3 increases *ca.* by 8 orders of magnitude. For this phospholipid, the gain was derived from the interaction of the phosphates with the Zn^{II} ions (*ca.* by 4/5 orders of magnitude, at least 4 charges) and the hydrophobic binding to the hydrocarbon portion of the passivating monolayer (more than 3 orders of magnitude). This is only possible because of the multivalency of the two interacting species (Fig. 5).

The potential application of cationic nanoparticles for the selective extraction of PIP3 from biological samples is evident. PIP3 is a crucial biomarker in lung inflammatory diseases and cancer, making its reliable quantification a basic requisite for early diagnosis. The available protocols[30] still remain challenging and rely on classical extraction of PI from a cell lysate, followed by radiolabeling or analysis by HPLC-MS. The use of AuNP **1**·Zn^{II} (or similar nanoparticles) could constitute an appealing, relatively simple approach.

Conflicts of interest

There are no conflicts to declare.

References

‡Very likely, upon interaction with the metal ions, the phosphates are further deprotonated, and hence more charges develop on the substrate.
§Control experiments showed that PIP3 is fully soluble in this solvent mixture.

1 M.-C. Daniel and D. Astruc, *Chem. Rev.*, 2004, **104**, 293–346.
2 L. J. Prins, *Acc. Chem. Res.*, 2015, **48**, 1920–1928.
3 L. Qin, G. Zeng, C. Lai, D. Huang, P. Xu, C. Zhang, M. Cheng, X. Liu, S. Liu, B. Li and H. Yi, *Coord. Chem. Rev.*, 2018, **359**, 1–31.
4 F. Manea, F. B. Houillon, L. Pasquato and P. Scrimin, *Angew. Chem., Int. Ed.*, 2004, **43**, 6165–6169.
5 H. Wei, L. Gao, K. Fan, J. Liu, J. He, X. Qu, S. Dong, E. Wang and X. Yan, *Nano Today*, 2021, **40**, 101269.
6 L. Gabrielli, L. J. Prins, F. Rastrelli, F. Mancin and P. Scrimin, *Eur. J. Org. Chem.*, 2020, 5044–5055.
7 Y. Lyu and P. Scrimin, *ACS Catal.*, 2021, **11**, 11501–11509.
8 J. Czescik, S. Zamolo, T. Darbre, F. Mancin and P. Scrimin, *Molecules*, 2019, **24**, 2814.
9 R. Bonomi, A. Cazzolaro, A. Sansone, P. Scrimin and L. J. Prins, *Angew. Chem., Int. Ed.*, 2011, **50**, 2307–2312.
10 S. Aoki and E. Kimura, *Chem. Rev.*, 2004, **104**, 769–788.
11 M. Shionoya, T. Ikeda, E. Kimura and M. Shiro, *J. Am. Chem. Soc.*, 1994, **116**, 3848–3859.
12 J. Czescik, F. Mancin, R. Strömberg and P. Scrimin, *Chem. – Eur. J.*, 2021, **27**, 8143–8148.

This journal is © The Royal Society of Chemistry 2023

Open Access Article. Published on 21 December 2022. Downloaded on 2/8/2026 4:38:49 PM.
This article is licensed under a Creative Commons Attribution-NonCommercial 3.0 Unported Licence.

13 C. A. Hunter and H. L. Anderson, *Angew. Chem., Int. Ed.*, 2009, **48**, 7488–7499.
14 G. Pieters, A. Cazzolaro, R. Bonomi and L. J. Prins, *Chem. Commun.*, 2011, **48**, 1916–1918.
15 C. Pezzato, B. Lee, K. Severin and L. J. Prins, *Chem. Commun.*, 2013, **49**, 469–471.
16 S. Neri, R. Pinalli, E. Dalcanale and L. J. Prins, *ChemNanoMat*, 2016, **2**, 489–493.
17 S. G. Martin and L. J. Prins, *Chem. Commun.*, 2016, **52**, 9387–9390.
18 F. della Sala, S. Maiti, A. Bonanni, P. Scrimin and L. J. Prins, *Angew. Chem., Int. Ed.*, 2018, **57**, 1611–1615.
19 G. Pieters, C. Pezzato and L. J. Prins, *Langmuir*, 2013, **29**, 7180–7185.
20 T. Graber, J. Thomas, E. Johnson, A. Gericke and E. E. Kooijman, *Biophys. J.*, 2018, **114**, 126–136.
21 E. J. Dickson and B. Hille, *Biochem. J.*, 2019, **476**, 1–23.
22 G. Di Paolo and P. De Camilli, *Nature*, 2006, **443**, 651–657.
23 G. R. V. Hammond and J. E. Burke, *Curr. Opin. Cell Biol.*, 2020, **63**, 57–67.
24 K. Mikoshiba, *J. Neurochem.*, 2007, **102**, 1426–1446.
25 R. J. Hunter, *Zeta Potential in Colloid Science: Principles and Applications*, AcademicPress, 1988.
26 S. Bhattacharjee, *J. Controlled Release*, 2016, **235**, 337–351.
27 M. R. C. Marques, R. Loebenberg and M. Almukainzi, *Dissolution Technol.*, 2011, **18**, 15–28.
28 H. T. Le, J. W. Lee, S. C. Park, J. W. Jeong, W. Jung, C. W. Lim, K. P. Kim and T. W. Kim, *Chem. Commun.*, 2017, **53**, 10459–10462.
29 O. Idevall-Hagren and P. D. Camilli, *Biochim. Biophys. Acta, Mol. Cell Biol. Lipids*, 2015, **1851**, 736–745.
30 *Phosphoinositides: Methods and Protocols*, ed. R. J. Botelho, Humana, New York, NY, 2021.